LA-UR-11-10334
Approved for public release; distribution is unlimited.

Title: Ray Tracing through the Edge Focusing of Rectangular Benders and an Improved Model for the Los Alamos Proton Storage Ring

Author(s): Kolski, Jeffrey S.
Barlow, David B.
Macek, Robert J.
McCrady, Rodney C.

Intended for: Report

Ray Tracing through the Edge Focusing of Rectangular Benders and an Improved Model for the Los Alamos Proton Storage Ring

Jeffrey S. Kolski[1]*, David B. Barlow[1], Robert J. Macek[1], Rodney C. McCrady[1]
[1]*Los Alamos National Laboratory, Los Alamos, NM, 87545*
(Dated: April 5, 2011)

LA-UR 11-
PSR 11-003
AOT-ABS 11-

Particle ray tracing through simulated 3D magnetic fields was executed to investigate the effective quadrupole strength of the edge focusing of the rectangular bending magnets in the Los Alamos Proton Storage Ring (PSR). The particle rays receive a kick in the edge field of the rectangular dipole. A focal length may be calculated from the particle tracking and related to the fringe field integral (FINT) model parameter. This tech note introduces the baseline lattice model of the PSR and motivates the need for an improvement in the baseline model's vertical tune prediction, which differs from measurement by .05. An improved model of the PSR is created by modifying the fringe field integral parameter to those suggested by the ray tracing investigation. This improved model is then verified against measurement at the nominal PSR operating set point and at set points far away from the nominal operating conditions. Lastly, Linear Optics from Closed Orbits (LOCO) is employed in an orbit response matrix method for model improvement to verify the quadrupole strengths of the improved model.

I. INTRODUCTION

This is the last tech note in a series of reports[1–6] about experiments to test and to verify the application of the orbit response matrix (ORM) method for model improvement[7] in the Los Alamos Proton Storage Ring (PSR). Even though the baseline linear lattice model of the PSR predicts the measured horizontal betatron tune, dispersion function, and betatron amplitude functions, as shown in Refs. [1, 3, 4] respectively, the baseline model predicts a vertical tune that differs form the measurement by .05. This result indicates an over focusing of the vertical beam motion in the baseline model. Three possible sources for this additional vertical focusing in the baseline model are investigated in this study for model improvement: the PSR quadrupoles, the fringe fields of the extraction septa, and the edge focusing of the horizontal rectangular benders. The focusing strengths of the quadrupoles are suspected because one popular method to modify the baseline model to obtain the measured tunes is to multiply the quadrupole strengths by a few percent[8]. The fringe fields of the extraction sept could be the cause of the addition vertical focusing because they are not included in the baseline model. Lastly, a second method to obtain the measured tunes from the baseline model is to tweak the edge angles of the PSR horizontal benders[9] and thus the edge focusing is also suspect. The focusing of each of these three accelerator element types was measured with a different experimental procedure.

The ORM method for model improvement was employed to compare the the quadrupole strengths of the PSR with the gradients in the baseline model[6]. In order to be confident that the ORM method could be applied to the PSR, the closed orbit (CO) measurement by the beam position monitors (BPMs) was thoroughly studied and reported in Ref. [1]. Also in Ref. [2], corrector magnet hysteresis was shown not to effect the CO measurement so that the magnet power supplies would not need to be ramped before every corrector kick in the ORM measurement. Measurements of the dispersion and beta functions were performed to verify an improved model[3, 4]. As reported in Ref. [6], Linear Optics from Closed Orbits (LOCO)[10] was applied to fit model parameters, including the quadrupole strengths, to the measured ORM. The LOCO fit indicated $\sim -2.5\%$ decrease in the defocusing quadrupole strength. The LOCO fitted model produced a vertical tune prediction that agreed with measurement but shifting the defocusing quadrupole strengths by -2.5% decreased the accuracy of the beta function prediction. Additionally, the decrease in defocusing quadrupole strength indicated by the LOCO fit was not observed in the controls set point, controls read back, or power supply current output, and 2.5% in the quadrupole strength is too large to be quadrupole magnet hysteresis[6]. Thus, it was concluded that the quadrupoles were not the cause of the over focusing in the vertical in the baseline model.

The fringe fields of the PSR extraction septa are observed by the circulating beam, which receives a kick every turn. The fringe fields of the extraction septa may be diagonalized into a superposition of magnetic multipoles, as in the Beth representation[11]. The most important multipole in this investigation is the quadrupole component, which may be calculated by a change in the measured tune. Beam measurements to characterize the

*Electronic address: jkolski@lanl.gov

magnetic multipole components of the PSR extraction septa fringe fields are reported in Ref. [5]. It was shown that the vertical tune difference between septa on and septa off was only .005. This is a factor of 10 less than the discrepancy between the measured vertical tune and the baseline model prediction. The extraction septa fringe fields are also not the cause of the additional focusing in the vertical of the baseline model. However, since the baseline model does not include effects from the extraction septa fringe fields, including the quadrupole component of the septa fringe fields in the baseline model is already an improvement, just not the smoking gun.

The last location where the baseline model's treatment of the vertical focusing may be different than the real machine is in the edge focusing of the PSR benders. This tech note reports the application of ray tracing as a means to investigate the edge focusing of the PSR benders.

This tech note is divided into the following sections: Sec. II, *Rectangular Dipole As A Transfer Matrix*, introduces the transfer matrix formalism for a rectangular dipole and the effects of both fringe field and edge focusing; Sec. III, *Baseline Model Comparison with Measurement*, introduces the baseline model and compares its predictions with measurements motivating and highlighting the requirements for an improved model; Sec. IV, *Ray Tracing Through The Edge Focusing*, describes the investigation of the rectangular dipole edge focusing using 3D magnetic field simulations and particle ray tracing; Sec. V, *Improved PSR model*, introduces the improved model of the PSR; Sec. VI, *Improved Model Compared with Measurement*, compares predictions of the linear lattice functions by the improved model with predictions from the LOCO fitted and baseline models as well as with measurements; Sec. VII, *Model Verification Experiments*, verifies the improved model by comparing linear lattice function predictions of the improved model with measurement at parameter set points far from nominal PSR operating conditions; Sec. VIII, *LOCO and the Improved Model*, now with a verified improved model LOCO will be employed in a ORM method for model improvement to verify the quadrupole strengths of the improved model, proving that the previous LOCO result of $\sim$−2.5% decrease in the defocusing quadrupole strength was due to fitting the quadrupole focusing and not the edge focusing (which is not an available fitting parameter) in LOCO; Sec. IX, restates the conclusions of this tech note.

II. RECTANGULAR DIPOLE AS A TRANSFER MATRIX

As shown in Fig. 1, the longitudinal edges of a rectangular dipole are not perpendicular to the reference trajectory as in the case of a sector dipole. The reference orbit makes an angle to the normal of the longitudinal edges of the rectangular dipole equal to half the bending angle of the rectangular dipole. The edge angle of

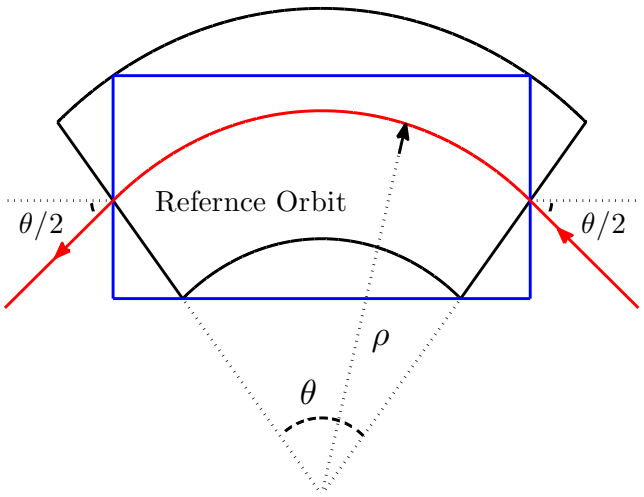

FIG. 1: Pictorial representation of the reference trajectory's (red) passage through a rectangular dipole, blue. The black solid line shows the geometry of a sector dipole.

the magnet produces both horizontal and vertical magnetic fields in the Frenet-Serrer coordinate system centered on the reference trajectory. The edge magnetic fields act as quadrupole lenses and give rise to the edge focusing. A rectangular dipole can be thought of as a sector dipole with thin lens quadrupoles on either side. Thus, the transfer matrix for a rectangular dipole may be written in terms of the quadrupole and sector dipole transfer matrices. The horizontal transfer matrix for a rectangular dipole is

$$\begin{aligned}\mathbf{M}_x &= \begin{pmatrix} 1 & 0 \\ \frac{1}{\rho}\tan\frac{\theta}{2} & 1 \end{pmatrix}\begin{pmatrix} \cos\theta & \rho\sin\theta \\ -\frac{1}{\rho}\sin\theta & \cos\theta \end{pmatrix}\begin{pmatrix} 1 & 0 \\ \frac{1}{\rho}\tan\frac{\theta}{2} & 1 \end{pmatrix} \\ &= \begin{pmatrix} 1 & \rho\sin\theta \\ 0 & 1 \end{pmatrix}, \end{aligned} \tag{1}$$

where ρ is the bending radius of the bend and θ is the angle of the bend. The focal length, f, of the edge focusing, which is here represented here as quadrupoles, is

$$f = \frac{\rho}{\tan(\frac{\theta}{2} - \zeta)}, \tag{2}$$

and may be found by geometrically relating the edge faces with respect to the reference trajectory of the rectangular dipole to the sector dipole. ζ is a correction term for the vertical focal length and is zero for the purposes of the horizontal edge focusing focal length. The horizontal transfer matrix for a rectangular dipole appears similar to the transfer matrix for a drift space of length $\rho\sin\theta$. In the transfer matrix equation of Eq. (1), the edge focusing of a rectangular dipole exactly cancels the focusing in the horizontal due to the bend and appears as a drift space in terms of the horizontal betatron motion. Physically, this is because the path length through a rectangular dipole, unlike a sector dipole, is independent of horizontal

Approximate Values for the Fringe Field Integral	
Hard Edge	0
Linear Field Decay	⅙
Clamped "Rogowski" Fringe Field	.4
Unclamped "Rogowski" Fringe Field	.7
"Square-Edged" Non-Saturating Magnet	.45

TABLE I: Common approximations of the fringe field integral for different magnetic field decay geometries[13].

position and each particle receives the same amount of bend.

The non-normal angle between the edge of the rectangular dipole magnet and the reference trajectory also acts to focus the vertical betatron motion. The vertical transfer matrix for a rectangular dipole magnet, like the corresponding horizontal transfer matrix, may also be written in terms of quadrupole and sector dipole transfer matrices,

$$\begin{aligned}\mathbf{M}_y &= \qquad (3)\\ &= \begin{pmatrix} 1 & 0 \\ -\frac{1}{\rho}\tan(\frac{\theta}{2}-\zeta) & 1 \end{pmatrix} \begin{pmatrix} 1 & \rho\theta \\ 0 & 1 \end{pmatrix} \begin{pmatrix} 1 & 0 \\ -\frac{1}{\rho}\tan(\frac{\theta}{2}-\zeta) & 1 \end{pmatrix} \\ &= \begin{pmatrix} 1-\theta\tan\left(\frac{\theta}{2}-\zeta\right) & \rho\theta \\ \frac{1}{\rho}\tan^2\left(\frac{\theta}{2}-\zeta\right)-\frac{2}{\rho}\tan\left(\frac{\theta}{2}-\zeta\right) & 1-\theta\tan\left(\frac{\theta}{2}-\zeta\right) \end{pmatrix}.\end{aligned}$$

The edge focusing of the rectangular dipole imposes additional focusing in the vertical betatron motion.

ζ is a correction term to the vertical focal length that takes into account the extent of the fringe fields[12] and the additional focusing due to those fringe fields,

$$\zeta = \frac{g\kappa}{\rho}\sec\left(\frac{\theta}{2}\right)\left(1+\sin^2\frac{\theta}{2}\right) \qquad (4)$$

where g is the full gap height of the dipole, ρ is the bending radius of the dipole, and κ is the fringe field integral also known as the FINT parameter in most modeling codes,

$$\kappa = \int_{-\infty}^{\infty} \frac{B_0 B_y(s) - B_y^2(s)}{gB_0^2} ds. \qquad (5)$$

In Eq. (5), B_0 is the constant dipole field at the center of the dipole magnet, and B_y is the vertical component of the magnetic field integrated along the reference trajectory. Common values for the fringe field integral for different end field geometries are posted in Tab. I.

III. BASELINE MODEL COMPARISON WITH MEASUREMENT

There are three accelerator models of the PSR described in this tech note. The first of which is what is named the baseline model. This model is called the baseline model because it represents the state of the model at the beginning of this model improvement endeavor; it is the default. The predictions of the baseline model are baseline predictions, where as the predictions from an improved model should enhance some model predictions but maintain at least the same quality as the baseline model for all predicted quantities.

The baseline model is basically an extension of F. Neri's DIMAD deck, *psrdimad.txt*[14], which in turn was a continuation of D. Johnson's SYNCH deck written during the direct H− injection upgrade, 1998. So the baseline model is based on a PSR model that was at least 8 years old prior to the beginning of this model improvement exercise. Thus, several modifications and extensions augmented F. Neri's model to construct the baseline model for this study.

The first complication was to assign the correct quadrupole magnet mapping dataset to the proper quadrupole. F. Neri's model contains current to gradient length conversions in the form of fourth order polynomial fits to the magnet mapping data described in Ref. [15] and recorded for posterity in Ref. [16]. The problem was that the magnet mapping data was labeled by quadrupole position in the PSR and not by magnet name or property number. It was also known that some of the quadrupoles had been relocated since the creation of F. Neri's model and the start of this investigation, let alone the time between the PSR commissioning (1986) and D. Johnson's SYNCH model in 2000. Thus, the first modification of F. Neri's model was to assign the quadrupole current to gradient length fits to the proper quadrupole by quadrupole name and then assign that quadrupole to the correct location in the PSR.

Following in the footsteps of D. Johnson, F. Neri defined the edge focusing of the rectangular PSR dipoles as thin lens quadrupoles with focal lengths $\frac{\rho}{\tan\theta/2}$ as in Eq. (1) for the horizontal, where $\theta/2$ is the edge angle of the rectangular bender. However, the effects of the fringe field focusing is not included in the vertical and Eq. (3) is applied as the vertical transfer matrix with $\zeta = 0$. The baseline model models the rectangular dipoles as rectangular dipoles with both edge and fringe field focusing, where the gap height and fringe field integral parameters are defined in Ref. [17].

Aside from the two modifications of F. Neri's model mentioned above, several additions were made to F. Neri's model to construct the baseline model. The first of these is that the locations of the dipoles and quadrupoles are determined from the 2006 alignment data[18]. The positions of the other elements in the lattice (the vertical correctors, the injection merging magnet RIBM09, and the foil) are determined by a combination of methods such as physical tape measurements and previous PSR models including S. Cousineau's[19], T. Spickermann's, and F. Neri's.

The vertical corrector magnets are also included in the baseline model. Constant current to kick conversations from Ref. [16] are assigned to the $7''$ and $11''$ vertical correctors. Although the PSR does not have dedicated

Measured and Baseline Model Tunes			
	Measured	Model	Error
Horizontal	$3.1915 \pm 4\times10^{-4}$	3.1973	-5.8×10^{-3}
Vertical	$2.1979 \pm 3\times10^{-4}$	2.2451	-4.7×10^{-2}

TABLE II: The baseline model predicted betatron tunes compared with measurement. The error in the model prediction is defined as measured minus model.

horizontal corrector magnets, zero length horizontal correctors are placed at the center of each of the PSR dipoles so that the baseline model may be compatible for use in an orbit response matrix analysis, Ref. [6]. Beam position monitors (BPMs) are also included in the baseline model for this same reason. As in the PSR, the model BPMs are placed 18 cm upstream of the center of each quadrupole.

Lastly, the baseline model is capable of reading magnet current and shunt input from a Save Accel data file. The Save Accel data file is a text file output by the controls system, which captures the state of the accelerator.

The predictions of the baseline model will be set as the standard for the improved model. The baseline model tune predictions compared with measurement are shown in Tab. II. While the baseline model predicts the horizontal tune well, the baseline model vertical tune prediction is not good at all. A model prediction of the vertical tune with error of .05 is just unacceptable. There is some amount of over-focusing in the vertical in the baseline model. There must be a vertical focusing element in the real machine that is not included in the baseline model, or the baseline model may not be properly handling a vertical focusing element. This is the motivation for an improved model of the PSR. The improved model of the PSR must produce a better vertical tune prediction.

The poor vertical tune prediction of the baseline model was expected because it existed in F. Neri's DIMAD deck. As mentioned before, there were two popular methods to correct for the model's vertical tune prediction. F. Neri adjusted the edge angles of PSR dipoles by about .8° to obtain the proper tunes[9]. The other method involved modifying the focusing and defocusing quadrupole strengths by a percent or so[8]. Both of these methods were quick fixes of changing a favored model parameter to obtain the measured vertical tune. No experiments were preformed to verify that either method was the correct modification.

Interestingly, the baseline model does a fairly good job at predicting the measured betatron amplitude functions[4] and the measured dispersion function[3]. Since the baseline model predicted beta functions agree with measurement, one might be lead to believe that the main source of focusing in the PSR (the quadrupoles) is handled properly. Another way to view the baseline model's performance compared to measurement is to compare the betatron phase at each BPM. (The results of the betatron phase measurement are discussed

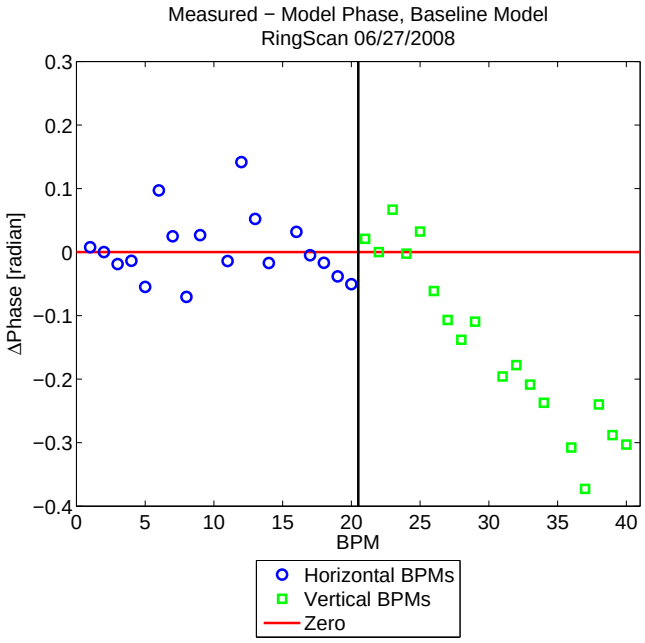

FIG. 2: (Color) The measured horizontal (blue circles) and vertical (green squares) betatron phase minus the baseline model prediction referenced to the betatron phase at the first BPM after the foil, SRPM02 (BPM 2 and 22). The red line marks zero, and the black line separates horizontal (left) and vertical (right) BPMs.

in Ref. [1]). Figure 2 plots the difference in the measured and model betatron phases referenced to the BPM 2 (SRPM02), the first BPM after the point of injection.

The horizontal phase comparison is very good, well within the measurement spread of .2 radians. However, there is room for some improvement in BPMs 5 through 13 since the error on the average of the fitted phase distribution at each BPM is only .02 radians.

Observe the systematic mistreatment of the phase advance in the vertical between BPMs starting at BPM 25. This systematic mishandling of the vertical phase starts in section 2 of the PSR right after the model encounters the first common 36° PSR bender. This may be an indication that the additional vertical focusing in the baseline model is located in the edge focusing of the common PSR benders.

The constant slope in the difference between the measured and model vertical phase is an indication that the vertical focusing error in the baseline model is not due to a single accelerator element (like a single misrepresented quadrupole strength) but a mistreatment of several like-elements, which combine to form the systematic mistreatment of the vertical phase shown in Fig. 2.

IV. RAY TRACING THROUGH THE EDGE FOCUSING

All of the horizontal bending magnets in the PSR are rectangular dipoles, so the beam is vertically focused as it enters and exits each dipole.

As introduced in Eq. (5), the edge focusing model of a dipole is determined by three independent parameters: the angle between the normal of the magnet edge and the reference trajectory (edge angle), the gap height of the dipole, and the fringe field integral. The edge angle and magnet gap height are physical quantities and can be measured with a ruler and protractor. The fringe field integral is a bit more elusive. The values of the fringe field integral in the baseline model are derived from a direct integration of the simulated 3D magnetic fields as per Eq. (5).

The baseline model includes effects of the edge focusing. Since the horizontal benders are rectangular dipoles, the edge angles in the baseline model are defined as one half of the total dipole bend angle. The gap height and fringe field integrals in the baseline model are derived from results of the 3D magnet field simulation results reported in Ref. [17].

As a means to check the edge focusing in the baseline model, parallel rays were traced through 3D magnetic field simulations of the PSR dipoles. Although the rays are traced through the same simulated 3D magnetic fields that produced the fringe field integral value applied in the baseline model, the ray tracing yields a focal length of the edge focusing, which is an independent measurement from the fringe field integral calculation. The focal length of the edge focusing derived may be compared to the direct calculation of the fringe field integral by combining Eqs. (2), (4), and (5).

The parallel rays were initially positioned on a transverse grid at the longitudinal center of the dipole. Rays initially placed at the center of the magnet only encounter the focusing effects of the downstream edge and not the total focusing of both rectangular dipole edges. The grid of rays spanned 4 cm in the horizontal and vertical with a ray every centimeter. So 25 parallel rays ranging between ±2 cm in the horizontal and vertical were traced through the downstream half of the PSR dipoles. All rays were given on-momentum velocities for the simulation. D. Barlow of AOT-RFE carried out the ray tracing simulations from a TOSCA 3D simulation of the PSR horizontal bending magnets. The results of the ray tracing simulation through each type of PSR bender are reported in Refs. [20–24].

The coordinate system of the simulation is locked to the center of the dipole. The axis of interest is the vertical axis, which is reported as is y-axis in the simulations. As depicted in Fig. 3, all of the parallel rays are initially aligned with the z-axis and perpendicular to the x-axis, which points out such that the rays are bent toward the −x-axis direction. The ray tracing simulation is iterated along the ray trajectory (s-axis) and records the ray's position every centimeter. The results of parallel ray tracing through a common 36° PSR bender are shown in Fig. 4.

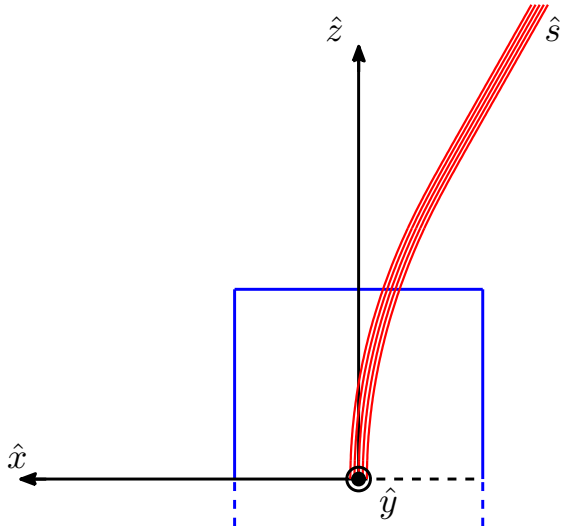

FIG. 3: (Color) Top-view cartoon schematic of the coordinate system used in the 3D magnetic field simulations. The ray traces are red and the magnet is shown in blue and the longitudinal coordinate, $\hat{s}$, is along the trajectory of the rays.

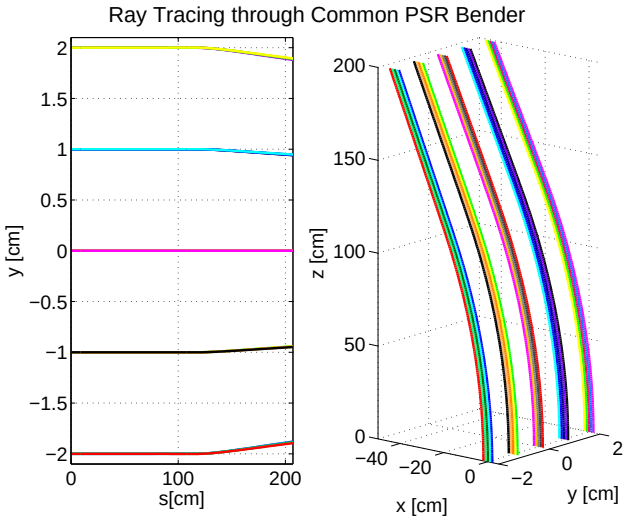

FIG. 4: The results of tracing parallel rays through a common PSR bending dipole. The left plot is a "side-view" along the ray's path showing the vertical focusing in the edge field, and the right plot graphs the rays in 3-space. Different colors represent rays with different starting positions.

The right plot of Fig. 4 shows the rays traced through the downstream half of a common PSR dipole and ∼.8 m of drift space in the 3D coordinate system of the simulation described above. The edge of the dipole is about −20 cm in x and 135 cm in z.

The left plot of Fig. 4 displays a ray's vertical position as a function of distance along the ray's trajectory,

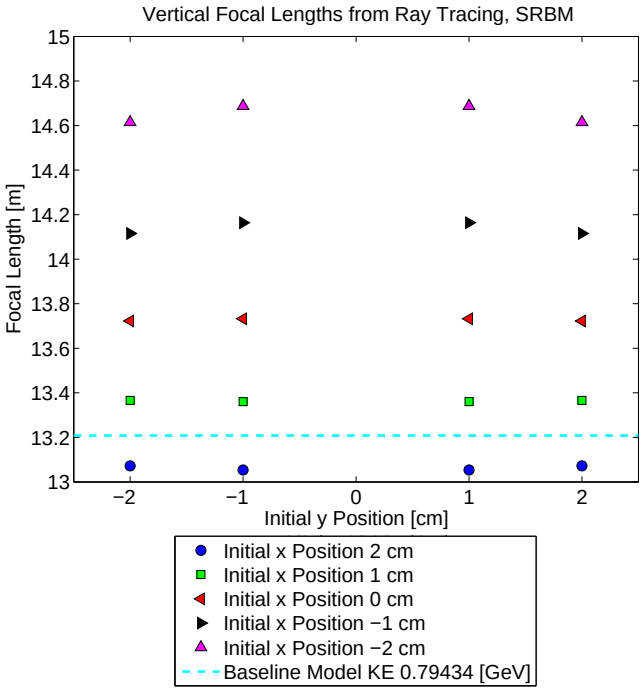

FIG. 5: (Color) The focal lengths calculated from rays traced through a common PSR bender with initial positions horizontal positions 2 cm (blue circles), 1 cm (green squares), 0 cm (red left pointing triangles), −1 cm (black right pointing triangles), and −2 cm, magenta up pointing triangles. The dashed cyan line is the focal length of the edge focusing from the baseline model at the momentum of the ray tracing simulation.

in the $\hat{s}$ direction. The edge of the dipole is around 130 cm on the s-axis. It is at this point that the rays with nonzero initial vertical position are focused due to the dipole edge focusing. As expected from the discussion of rectangular dipoles in Sec. II, the edge focusing provides a quadrupole-like focusing affect in the vertical with focusing strength depending linearly on vertical position. This is observed in Fig. 4 because the rays with initial vertical position of ±2 cm are bent about twice as hard as the rays with ±1 cm initial vertical position.

The focal length of the edge focusing maybe calculated from the ray tracing data. A line, $y(s)$, is fit by linear regression to the bent trajectory of the ray, roughly the portion of the ray between $s = 140$ and the end of the ray tracing. The focal length for the focusing of the ray is then the location in s where the fitted line equals zero minus the location in s where the fitted line equals the initial vertical position (where the ray receives the angular kick from the edge focusing). The calculated focal lengths from tracing rays though a common PSR bender are shown in Fig. 5.

The rays with initial vertical positions of zero are not focused because they propagate through the center of the quadrupole-like edge focusing field and thus lead to focal lengths of zero. For each initial horizontal starting position, the focal lengths are symmetric about the 0 cm initial vertical position. Notice that the focal length varies across the grid of initial positions. This magnetic aberration is small for a given initial horizontal position and is expected in real magnets. Note that the grid of initial positions extends to ±2 cm, further than the calibrated region of the BPM measurement, and much further than where the CO is located during typical operations.

The focal lengths resulting from the ray originating from initial horizontal position 0 cm and initial vertical position ±1 cm should be compared with the focal length of the edge focusing in the baseline model. Figure 5 shows that the model edge focusing focal length is about half a meter shorter than the focal length resulting from the ray tracing data. A shorter focal length indicates stronger vertucal focusing and a larger betatron tune.

The focal length of the edge focusing resulting from the ray tracing simulations may be constrained in an improved model by altering any one or all of the three parameters that affect the edge focusing: edge angle, gap height, and fringe field integral. For simplicity only one of the parameters will be modified to impose the focal length results from the ray tracing simulation in the improved model.

The baseline model value for the edge angle may be incorrect because the edge angle should really be between the normal of the magnetic field gradient and the reference trajectory. Since the main coils of the PSR bending magnet extend further longitudinally than the iron, the magnetic field gradient and the edge of the magnet may not be parallel. However, the edge angle will not be modified to constrain the model edge focusing focal length because inverting Eq. (4) for θ results in a transcendental equation.

The baseline model value for the magnet gap height may be incorrect because the gap is not constant transversely and because there are shims at the magnet ends, which reduce the gap height. The shims are in place to limit higher order magnetic multipoles. Since imposing the focal lengths from the ray tracing can modify the gap height by several centimeters, it is not chosen as the model parameter to modify for constraining the edge focusing focal length.

The fringe field integral is chosen somewhat arbitrarily as the parameter to constrain in order to impose the focal length results of the ray tracing simulation in the improved model. A comparison of the focal lengths and associated fringe field integrals for the different PSR horizontal bender types and models is shown in Tab. III.

The largest fractional difference in the edge focusing focal length occurs for the common PSR benders. Modifying the common PSR dipole edge focusing focal length has the most effect on the model vertical tune. There are several reasons for this: one, most of the PSR benders are the common 36° dipoles, two, the common PSR dipoles have the largest bend angle of the horizontal benders (recall that the focal length of the edge focusing is

Fringe Field Integrals and Corresponding Focal Lengths Employed in the Baseline and Improved Models				
Magnet	Focal Length [m]		Fringe Field Integral	
	Baseline	Improved	Baseline	Improved
Common	13.208	13.733	.54150	.90291
SRBM01	13.208	13.733	.54150	1.2908
SRBM11	32.186	32.389	.44940	.46491
SRBM12	30.823	30.889	.51930	.52685
RIBM09	234.17	238.96	.35790	.47085

TABLE III: The focal lengths and fringe field integrals for each type of PSR horizontal bender employed in the baseline model (found by direct calculation of the fringe field integral in 3D magnetic field simulations) and the improved model, found by ray tracing through simulated 3D magnetic fields.

inversely proportional to the tangent of half the bending angle, Eq. (2)), and three, the edge focusing focal lengths are shortest for the common dipoles. The ray tracing results suggest a dramatic modification to the fringe field integral for the common PSR benders. However, a fringe field integral of .90291 is more representative of the unclamped "Rogowski" type geometry of the common PSR benders, Tab. I.

The ray tracing data suggests the largest change in the edge focusing focal length at RIBM09. However, this modification has little effect on the model vertical tune prediction because the edge focusing from RIBM09 is so weak due to a small bend angle of 6.8°, and the resulting focal length is almost three times the circumference of the PSR.

Interestingly, the ray tracing results suggest that there is a very small additional horizontal focusing element in the edge focusing of the PSR benders. The horizontal focal length was found to be greater than 300 m and was not included in the improved model. This result indicates that the PSR benders are really rectangular dipoles with an edge angle equal to one half of the total bend angle such that the horizontal focusing of the sector dipole is completely canceled by the edge focusing.

The focal length results from ray tracing simulations are systematically longer than the focal lengths from the baseline model indicating an over focusing in the vertical at all of the PSR benders. This provides for the systematic mistreatment of the vertical phase advance observed in Fig. 2. Observe that the difference in measured and model vertical phase in Fig. 2 seems random and about the same amplitude as the horizontal difference in phase until BPM 26. BPM 26 (SRPM22) is the downstream BPM in section 2, the section immediately after the first common PSR dipole encountered after the foil. From this point onward, there is a systematic mistreatment of the model vertical phase advance, observed in Fig. 2 as a constant drift negative. It is interesting that this should coincide with the location of the first common PSR bending magnet encountered after the foil.

Note the magnitude of the fringe field integral parameter for SRBM01 in the improved model in Tab. III. SRBM01 is a common 36° bender but is operated at 100 A less than the other common PSR benders in order to bend the beam only 32.8°, which allows "room" for the merging magnet, RIBM09. A fringe field integral greater than one would suggest that the vertical component of the magnetic field in the fringe field would change sign. It is hard to understand how this could be, but it is a complicated situation since the main coils of SRBM01 extend longitudinally well past the iron. Perhaps the normal of the gradient of the magnetic field is at a different angle than the iron such that SRBM01 is not really a rectangular dipole. Nonetheless, the accelerator toolbox (AT) model is able to handle a fringe field integral parameter greater than one, and the model is constrained to produce the same focal length in the edge focusing as observed in the ray tracing data.

The difference between the focal lengths from the 3D magnetic field integral calculation and the constrained focal lengths from the ray tracing has not been resolved. The same magnetic fields from the TOSCA simulation were applied in both calculations. Could it be that the K. Brown[12] model for the edge focusing applied in the AT program (Eqs. (4) and (5)) is not the correct model for the PSR dipoles? The assumptions made in the derivation of Eqs. (4) and (5) should be understood and checked against the situation in the PSR. The mechanics of the edge focusing of the PSR benders should be investigated

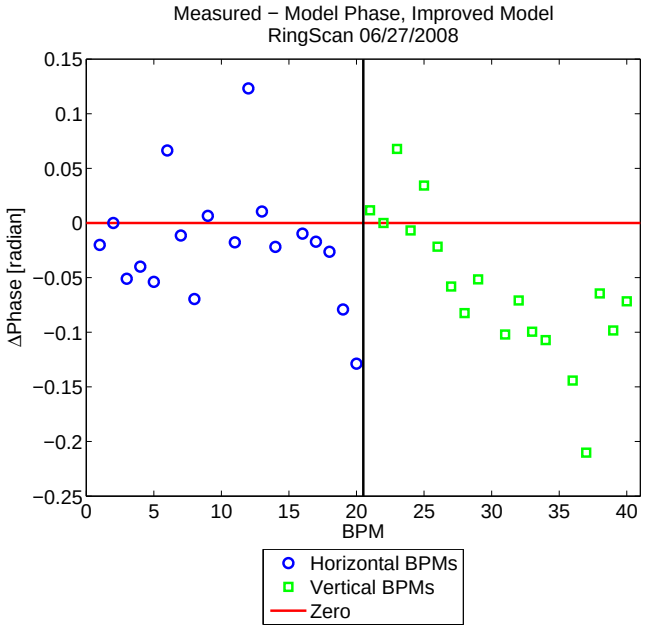

FIG. 6: (Color) The measured horizontal (blue circles) and vertical (green squares) betatron phase minus the improved model prediction referenced to the betatron phase at the first BPM after the foil, SRPM02. The red line marks zero and the black line separates the horizontal (left) and vertical (right) BPMs.

further in the future. Nonetheless, the model focal length of the edge focusing from each PSR dipole may be constrained to the same as the focal lengths observed from the ray tracing. This modification to the baseline model improved the treatment of the vertical phase advance as observed in Fig. 6.

Figure 6 shows the difference in the measured betatron phase and the phase predicted from an improved model with edge focusing constrained to the values indicated by the ray tracing data. Comparing Fig. 6 with Fig. 2, it is easy to see that the ray tracing derived edge focusing focal lengths produce better predictions of the vertical phase. Note that the systematic mistreatment of the vertical phase has been reduced to the same level of error as the horizontal phase. However, it is still possible to observe a slight negative drift in the vertical phase difference. This indicates, that although the major source of error has been identified, refinement is still possible.

One also needs be careful when calculating the focal length from the ray tracing data as to make sure to find the focal length with respect to the coordinate along the beam trajectory ($\hat{s}$) and not the initial longitudinal direction of the simulation, $\hat{z}$. If the focal length of the edge focusing is found along the z-direction, the focal lengths in the baseline model are obtained. The difference between $\hat{s}$ and $\hat{z}$ is greatest for the case of the common PSR benders because their bending angle is the greatest.

V. IMPROVED PSR MODEL

An enhanced model of the PSR may be created by considering the results of the model improvement experiments documented in Refs. [5, 6], the lattice function measurements described in Refs. [1, 3, 4], and the results of the ray tracing simulations. The improved model of the PSR is founded on the baseline model discussed in Sec. III. All considerations made in the baseline model are also in the improved model. However, the improved model benefits from the experimental results described in Refs. [5, 6], where as the baseline model does not. The combined results of the ORM[6], extraction septa characterization[5], and ray tracing through the dipole edge focusing (Sec. IV) indicate the presence of two types of vertical focusing elements in the real machine that are not handled properly in the baseline model of the PSR.

The LOCO fitted quadrupole strengths are not included in the improved model because the LOCO fitted model was not able to predict the betatron amplitude functions as well was the baseline model[6].

The PSR extraction septa characterization experiment measured the quadrupole component of the fringe fields of the extraction septa. The circulating beam observes these quadrupole focusing fields and receives the appropriate kick each revolution. Although the quadrupole fields of the septa fringe fields were found to be about .1 the strength of the PSR quadrupoles, the septa fringe fields were observed to modify the betatron tune by .005, which is about the prediction accuracy hoped for in the tune by the improved model. Thus, the improved model enhances the baseline model with the inclusion of the quadrupole component of the PSR extraction septa fringe fields.

The septa fringe fields are modeled as thin quadrupoles located at the upstream outer corners of the exaction septa. The model makes use of the measured and fit extraction septa trim coil current to magnetic moment strength from the septa characterization experiment. Thus, the septa fringe fields are modeled operationally. The improved model reads the Save Accel file containing the septa trim coil current, consults the four order current to gradient length fit calculated in Ref. [5], and defines a thin lens quadrupole with corresponding focal length.

The second modification between the baseline and improved PSR models is the handling of the edge focusing of the horizontal rectangular dipole magnets. The ray tracing through the PSR dipoles reveals focal lengths for the edge focusing different from those applied in the baseline model. The difference in the focal lengths is only about .5 m in the common PSR benders but this is enough to lower the model predicted tune to measured values. The focal lengths measured in the ray tracing experiment are ensured in the improved model by constraining the fringe field integral. The difference in the fringe field integral parameter and resulting edge focusing focal length between the baseline and improved models is shown in Tab. III.

VI. IMPROVED MODEL COMPARED WITH MEASUREMENT

As with the LOCO fitted model in Ref. [6], the improved model must be shown to enhance the predictions of the baseline model in comparison to measured quantities before it is heralded as a better model. The baseline and improved models of the PSR are linear lattice models, so the predicted quantities of interest are the betatron tunes, betatron amplitude functions, and the dispersion function. The comparisons of the baseline and improved models with the measured tunes, beta functions, and dispersion function are displayed in Tab. IV.

The betatron tune comparison between improved model prediction, baseline model prediction, and measurement is easy because the tune is a single number. Thus, a simple difference (prediction error) between the model prediction and measurement is employed to compare the predictions of the models.

It is a little harder to compare the other lattice functions of interest (betatron phase, beta functions, and dispersion function) because they are vectors of numbers with a measured or predicted quantity at each BPM. Simply subtracting and averaging vectors of data is not the best manner of comparing when each vector element possesses a different measurement error. Thus, each vec-

Comparison of Measured and Model Predicted Linear Lattice Functions			
	Baseline	LOCO Fitted	Improved
Betatron Tune: rms Measurement Spread [3.447×10^{-4}, 3.238×10^{-4}]			
Horizontal Error	−.005840	.00457	−.01210
Vertical Error	−.04716	−.03868	−.007477
Betatron Phase: Mean Measurement Spread [.20 mradian, .18 mradian]			
Total χ^2/DOF	0.700	0.397	0.189
Horizontal χ^2/DOF	0.072	0.088	0.084
Vertical χ^2/DOF	1.328	0.707	0.294
Beta Function: Mean Systematic Error, Large Beta [.4960 m, .4035 m] Mean Systematic Error, Small Beta [.0504 m, .1153 m]			
Total χ^2/DOF	12.770	13.321	12.025
Horizontal χ^2/DOF	20.928	21.932	18.553
Vertical χ^2/DOF	4.611	4.710	5.496
Dispersion Function: Mean Fitting Error .05564 m			
χ^2/DOF	24.543	20.014	17.272

TABLE IV: The baseline, LOCO fitted, and improved model predictions compared to the measured betatron tunes and phase (from the RingScan reproducibility dataset[1]), betatron amplitude functions (quadrupole perturbation method[4]), and the dispersion function (α_c method[3]). The *rms* measurement spread, systematic error, and fitting error were applied in the χ^2 calculations comparing the phase, beta function, and dispersion functions respectively.

tor element is weighted by its measurement error in a χ^2/DOF comparison between the measured and model predicted vectors of the betatron phases, beta functions, and dispersion functions. The χ^2/DOF comparison is employed to quantify the goodness of the model predictions. There is no fitting in this comparison between the measured and model predicted lattice functions. The χ^2 is employed as a means to compare two vectors of data. For the betatron phase comparison, the measurement spread at each BPM is employed as the error in χ^2 calculation. However statistically improper, the systematic error due to the uncertainty in the quadrupole current to gradient length conversions on the measured beta functions is applied as the error in the χ^2 calculation for the beta function comparison because it was the dominating uncertainty[4]. Lastly, the fitting error on the dispersion function is applied as the error in the χ^2 calculation comparing the model predicted and measured dispersion functions.

The measured data compared in Tab. IV is collected from three different measurements during two different development periods. The betatron tunes and betatron phases are from the RingScan reproducibility dataset taken during the July, 26, 2008 accelerator development discussed in Ref. [1]. The *rms* spread of the fitted phase parameter at each BPM is applied in the calculation of the χ^2/DOF. The measurement spread is employed instead of the error on the average phase to wash out possible affects of running the models at a different energy than the measured data was taken. The beta functions were measured with the quadrupole perturbation method also during the July, 26, 2008 accelerator development and are discussed in Ref. [4]. The systematic error on the beta function measurement due to the uncertainty of the quadrupole current to gradient length conversion is the dominating error in the measurement and is thus applied, however statistically incorrect, in the χ^2 calculation for the beta functions. Lastly, the measured dispersion function compared with the models in Tab. IV is from the December 22, 2009 accelerator development dataset and was measured with the α_c method, Ref. [3]. The dispersion function χ^2 calculation employs the fitting error on the dispersion function. The results of the LOCO fitted model are repeated here from Ref. [6] for convenience of comparison.

The first test of the improved model will be whether it predicts the measured betatron tunes more accurately than the baseline model. The first thing to note in Tab. IV is that the improved model's vertical tune prediction is closer to the measured value by .04 compared to the baseline model. In other words, the improved model has corrected the deficiency in the baseline model's vertical tune prediction. One may note that the improved model predicts a much better vertical tune at a slight expense of the horizontal tune prediction. It is a little disappointing that the improved model predicts a horizontal tune with error twice as large as the baseline model, however, this may be effects of as quadrupole hysteresis. The model predicted betatron phase at each BPM compared with measurement should be consulted to quantify the worsening of the horizontal tune prediction by the improved model.

Although the baseline model yields a small χ^2/DOF when compared to the measured horizontal betatron phase, the improved model makes a more accurate overall prediction, specially in the vertical. Observe in the horizontal and vertical breakdowns of the total betatron phase χ^2 comparison that the horizontal χ^2 is slightly larger for the improved model but less than the LOCO fitted model χ^2. This is representative of the increased error on the horizontal tune prediction by the improved model. However, the slightly less accurate horizontal phase prediction by the improved model is greatly made up in the much smaller vertical χ^2 yielding a smaller total χ^2/DOF when considering all betatron phase predictions. This indicates that over all, the improved model does a better job at predicting the betatron tunes than the baseline model.

The slightly larger error in the improved model's horizontal tune prediction is not very troublesome after all. Additionally, there is the consideration that the PSR quadrupoles were not ramped prior to the RingScan reproducibility measurement. Thus, magnet hysteresis may play a considerable role in the $\sim$.01 horizontal tune

error[4] of the improved model. However, if the improved model consistently yields a horizontal tune prediction .01 off from measured, the improved model may possess its own deficiencies. Keep this in mind during the model verification experiments discussion in Sec. VII.

Thus, it is necessary to conclude that the improved model passes the first test of model enhancement, the improved model's prediction of the betatron tunes enhances the prediction capabilities of the baseline model.

The second test to prove that the improved model is better than the baseline model and the correct linear model to be applied to the PSR is the prediction of the betatron amplitude functions. According to the results posted in Tab. IV, the improved model enhances the horizontal beta function prediction while slightly decreasing the accuracy of the vertical beta function prediction. It is interesting that the improved model should yield a much better vertical tune prediction while yielding a slightly worse beta function prediction in the vertical. One may believe the quality of these two parameters to be more correlated. However, the best overall beta function prediction goes to the improved model. Thus, the improved model also passes the second test to prove it is a better model than the baseline model. Recall that the LOCO fitted model was not established as an improved model because it was not able to predict the beta functions as well as the baseline model[6].

It is interesting to note that of the modifications applied to create the improved model from the baseline model, only the quadrupole component of the extraction septa fringe fields effects the horizontal focusing lattice. The edge focusing of the rectangular dipoles only focuses vertically. Thus, the large improvement in the horizontal beta function as shown in the χ^2 comparison of Tab. IV is solely due to the inclusion of the PSR extraction septa focusing fringe fields.

The last comparison in Tab. IV is the dispersion function. While not necessarily a test of model improvement, the dispersion function is a linear lattice function, which should be predictable by a good model of the PSR. The dispersion is defined by all of the previously compared machine parameters, i.e. beta functions and phase advances. And as expected, the improved model produces the better dispersion function prediction because it produces superior predictions of the horizontal betatron amplitude and phase functions.

Thus, with the comparisons in Tab. IV made, the improved model has shown that it is actually an enhancement of the baseline model for these measurements of the betatron tunes, phases, amplitude functions, and dispersion functions at this set point for the PSR.

VII. MODEL VERIFICATION EXPERIMENTS

Now that the improved model has been shown to be a better model for the PSR than the baseline model at a particular set point, the improved model needs to be tested far away from the nominal operation set point in order to verify its superiority to the baseline model. Three RingScan reproducibility datasets were collected during the September 25, 2010 accelerator development to verify the quality of the improved model. Each RingScan reproducibility dataset was taken at different PSR quadrupole settings yielding different tunes and beta functions compared to normal operations. The quadrupole power supplies were ramped to maximum before the collection of each reproducibility dataset to ensure that the quadrupoles operated on the top hysteresis curve where the magnet mapping occurred.

Due to a shortage of remaining development time, fifty RingScans instead of the nominal 100 RingScan were collected during each reproducibility measurement. Likewise, the CO was centered, the injection offset lowered to near-on-axis, and the energy was corrected for the first reproducibility dataset, but to save time this set up procedure was not performed for the second or third datasets.

The baseline and improved models produce tunes and betatron phases for direct comparison with results from the RingScan reproducibility measurements. Comparing the model predicted beta and dispersion functions directly with the fitting parameters from the turn-by-turn RingScan data is a little more difficult because the quadrupole perturbation method was not employed to measure the actual betatron amplitude functions nor were momentum measurements made to measure the real dispersion function. However, the model predicted beta and dispersion functions may still be compared with measurement, even if the actual beta and dispersion functions were not measured directly. The beta function may be inferred from the fitted amplitude, and the dispersion function may be related to the horizontal CO measurement spread.

The measured (fitted) amplitude of the betatron oscillation may be related to the model predicted beta functions by

$$A(s) = \sqrt{2J\beta(s)}, \tag{6}$$

where A is the amplitude of the betatron oscillation, the action J is determined by the injection offset, β is the betatron amplitude function, and s in the longitudinal coordinate. In this case the action must be fit. Linear regression will serve well for the fit of the action. This is a one parameter fit, so the χ^2/DOF comparing the model predicted beta functions and the fitted amplitudes from the RingScan data has one less degree of freedom than the number of BPMs.

Likewise, the fitted offset *rms* measurement spread can be related to the model predicted dispersion function by[1]

$$\sigma_{CO}^2 = \sigma_{BPM}^2 + 2D\langle\epsilon_{BPM}, \epsilon_\delta\rangle + D^2\sigma_\delta^2, \tag{7}$$

where σ_{CO} is the total CO measurement spread, σ_{BPM} is the intrinsic BPM measurement spread, σ_δ is the magnitude of the pulse-to-pulse momentum spread, $\langle\epsilon_{BPM}, \epsilon_\delta\rangle$

is the covariance between the errors due to the momentum variation (ϵ_δ) and the BPM measurement error (ϵ_{BPM}), which is expected to be small. Like for the beta function comparison, the model dispersion function must be fit to the CO measurement spread by Eq. (7). In order to save one degree of freedom, the BPM measurement error may be constrained to equal the intrinsic BPM resolution, .02 mm. Linear regression is employed to fit for the covariance between the momentum and BPM error and the magnitude of the pulse-to-pulse momentum variations. The sum of squares of residuals (SSR) is applied as the statistic to compare the model and "measured" dispersion functions because the uncertainty on the CO measurement spread is unknown, thus the χ^2 is undefined. The SSR/DOF which compares the model to measurement has two less degrees of freedom than the number of BPMs.

The measurements from the first RingScan reproducibility dataset with tunes [3.2266, 2.2192] are compared with results from the baseline and improved models in Sec. VII A, data from the second reproducibility dataset with tunes [3.8002, 2.3826] is discussed in Sec. VII B, and lastly, the comparison of the third dataset with tunes [2.6539, 3.5829] is shown in Sec. VII C.

Comparison of Model and Measured RingScan data and, $\nu_x = 3.2266$, $\nu_y = 2.2192$		
	Baseline	Improved
Betatron Tune: rms Measurement Spread [8.763×10^{-4}, 3.927×10^{-4}]		
Horizontal Error	.004154	.0006517
Vertical Error	−.03591	.002878
Betatron Phase: Mean Measurement Spread [.037 mradian, .017 mradian]		
Total χ^2/DOF	86.112	19.929
Horizontal χ^2/DOF	5.561	4.308
Vertical χ^2/DOF	166.663	35.549
Beta Function: Mean Meas. Spread, Large Amp. [.3201 mm, .1785 mm] Mean Meas. Spread, Small Amp. [.1369 mm, .0896 mm]		
Total χ^2/DOF	3.636	3.484
Horizontal χ^2/DOF	3.395	3.361
Vertical χ^2/DOF	3.878	3.608
Dispersion Function:		
SSR/DOF	.003139	.003153

TABLE V: The baseline and improved model predictions compared to the results of the RingScan analysis. The *rms* measurement spread is applied in the χ^2 calculations for the phase and beta functions.

A. Reproducibility 1 with tunes [3.2266, 2.2192]

The first reproducibility dataset was collected at the production operating set point found at the beginning of the September 25, 2010 development period. The CO was centered, the injection offset lowered to [−3.313 mm, .456 mradian] in the horizontal and [2.168 mm, .847 mradian] in the vertical. The energy was corrected. The quadrupole power supplies were ramped, the magnets allowed to saturate at maximum, and the currents were brought down to their production set points. The focusing quadrupole power supply (BEMP02) was set to 462.8 A, and the defocusing quadrupole power supply (BEMP03) was set to 282 A. The measured betatron tunes for these quadrupole settings are [3.2266, 2.2192]. These tunes are a bit high for nominal PSR production, but it is how the machine was running during the September 2010 production run. The baseline and improved model predictions are compared with the results of the RingScan measurement in Tab. V.

The improved model produces closer predictions than the baseline model for all cases in Tab. V. The improved model reduces the error on the tune prediction by about a factor of ten compared to the baseline model. Also note the slight increase in the improved model's horizontal tune prediction observed in Tab. IV is not shown in Tab. **??**. This indicates that the improved model does produce a superior horizontal tune prediction and that the cause for the slight increase in Tab. IV is most likely due to quadrupole hysteresis.

The enhanced tune predictions by the improved model are also indicated in the betatron phase comparison. Although the error on the tune prediction by the improved model is about ten times better, the χ^2/DOF in the horizontal phase comparison is only slightly improved. The χ^2/DOF for the phase comparisons are much larger than those displayed in Tab. IV. This is because the large amplitudes of betatron oscillation are about 8 mm, which produces less spread in the phase measurement compared to the few millimeter amplitude from the RingScan reproducibility measurement discussed in Ref. [1] and compared with measurement in Tab. IV. The smaller measurement spread calculates a larger χ^2/DOF for the same residual between predicted and measured.

Likewise, the increased amplitude also increases the amplitude measurement spread which dramatically lowers the χ^2 in the betatron amplitude comparisons. The baseline model has always performed well in its beta function prediction. Remember that the LOCO fitted model was discounted because the baseline model's beta function prediction was superior[6]. However in the beta function prediction, the improved model again surpasses the baseline prediction.

B. Reproducibility 2 with tunes [3.8002, 2.3826]

The second RingScan reproducibility dataset was collected with the focusing quadrupole power supply BEMP02 set at 522 A and the defocusing quadrupole power supply BEMP03 set at 312.1 A. These quadrupole settings yielded a measured tune of [3.8002, 2.3826]. This places the horizontal tune on the other side of the half integer, but like the .2 fractional tune case, there are

Comparison of Model and Measured RingScan data and, $\nu_x = 3.8002$, $\nu_y = 2.3826$		
	Baseline	Improved
Betatron Tune: rms Measurement Spread [2.231×10^{-3}, 3.481×10^{-4}]		
Horizontal Error	.01169	.005775
Vertical Error	−.04135	−.002603
Betatron Phase: Mean Measurement Spread [.185 mradian, .021 mradian]		
Total χ^2/DOF	37.870	4.736
Horizontal χ^2/DOF	1.741	1.931
Vertical χ^2/DOF	74.000	7.540
Beta Function: Mean Meas. Spread, Large Amp. [.2704 mm, .2301 mm] Mean Meas. Spread, Small Amp. [.0673 mm, .1198 mm]		
Total χ^2/DOF	3.140	2.244
Horizontal χ^2/DOF	0.278	0.235
Vertical χ^2/DOF	6.001	4.252
Dispersion Function:		
SSR/DOF	.002806	.002657

TABLE VI: The baseline and improved model predictions compared to the results of the RingScan analysis. The *rms* measurement spread is applied in the χ^2 calculations for the phase and beta functions.

still ∼5 turns per betatron oscillation at the fixed location of the BPM. The injection offset for this measurement was [−.05868 mm, .05271 mradian] in the horizontal and [2.431 mm, .9848 mradian] in the vertical. The tiny horizontal injection offset leads to a larger spread in the horizontal tune measurement. The horizontal CO was also dramatically modified due to the change in the quadrupole power supplies, with COs larger than 10 mm. The comparison of the improved model lattice function predictions with the baseline model predictions and measurement is provided in Tab. VI.

Again the improved model proves to possess superior predictive capabilities compared to the baseline model in predicting the tune and beta functions. The slight increase in the horizontal phase χ^2 for the improved model compared to the baseline model is not worrisome because of the much better horizontal tune prediction. Additionally, the horizontal phase measurement spread is large because of the very small injection offset.

It should be noted that the χ^2/DOF reported in Tab. VI can not be compared with the χ^2/DOF reported in Tabs. IV and V because the measurement spread of the measured linear lattice functions is different for each case. It can be assumed that the over all difference between the measured and modeled predicted quantities is more or less the same for each quadrupole power supply setting and that it is the measurement spreads which differ and weight the difference differently in the χ^2 calculation for each tune setting.

C. Reproducibility 3 with tunes [2.6539, 3.5829]

The last RingScan reproducibility dataset was taken with both quadrupole power supplies (BEMP02 and BEMP03) set to 421.8 A. The measured betatron tunes for these quadrupole set points were found to be [2.6539, 3.5829]. Note how this quadrupole setting switched the horizontal and vertical integer tunes. The injection offset was [.01013 mm, .09992 mradians] in the horizontal and [−1.600 mm, −.4297 mradian] in the vertical. Unfortunately, this quadrupole power supply setting resulted in a very small injection offset in both planes, but because the quadrupole strengths were so large, significant amplitudes were still achieved in each direction. The comparison of the improved model with the baseline model and measurement is provided in Tab. VII.

This quadrupole setting took the PSR furthest from its production set points. The comparison of the improved model with the baseline model and measurement is provided in Tab. VII. Even so, the improved model produces better tune predictions than the baseline model. However, it appears that the baseline model does a better job at predicting the beta functions. This is most likely a result of the RingScan measurement and not because the model prediction is bad.

The beta function comparison is shown in Fig. 7. The measured vertical amplitudes are erratic in nature. The largest surprises in the vertical amplitude measurement are at BPMs 26 and 28. These are BPMs in defocusing quadrupoles, so the betatron amplitudes should be large. However, the amplitudes at these BPMs are much

Comparison of Model and Measured RingScan data and, $\nu_x = 2.6539$, $\nu_y = 3.5829$		
	Baseline	Improved
Betatron Tune: rms Measurement Spread [1.178×10^{-3}, 1.050×10^{-3}]		
Horizontal Error	.01019	.006852
Vertical Error	−.03425	.005665
Betatron Phase: Mean Measurement Spread [.044 mradian, .016 mradian]		
Total χ^2/DOF	60.727	12.483
Horizontal χ^2/DOF	2.276	1.480
Vertical χ^2/DOF	119.178	23.486
Beta Function: Mean Meas. Spread, Large Amp. [.2367 mm, .1404 mm] Mean Meas. Spread, Small Amp. [.0974 mm, .0768 mm]		
Total χ^2/DOF	136.582	147.902
Horizontal χ^2/DOF	3.802	4.168
Vertical χ^2/DOF	269.361	291.636
Dispersion Function:		
SSR/DOF	.001822	.001841

TABLE VII: The baseline and improved model predictions compared to the results of the RingScan analysis. The *rms* measurement spread is applied in the χ^2 calculations for the phase and beta functions.

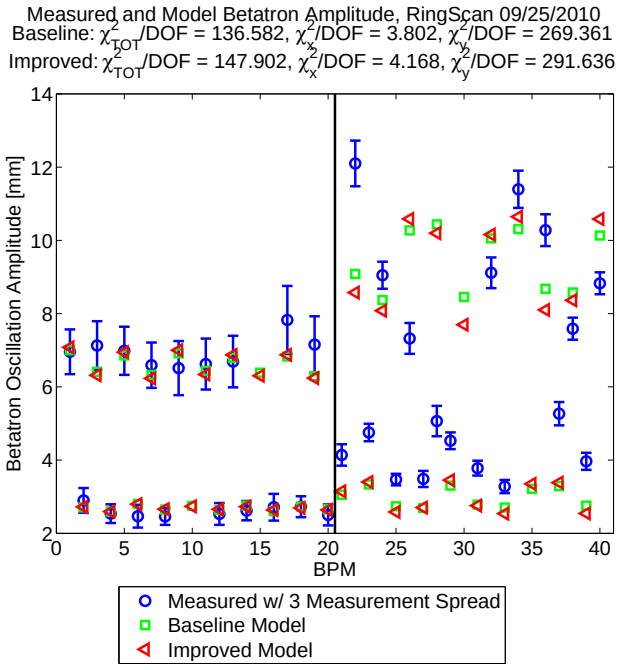

FIG. 7: (Color) The measured amplitude from the RingScan 3 dataset with three *rms* measurement spreads (blue circles) and the beta function predictions from the baseline (green squares) and improved (red left pointing triangles) models multiplied by the fit action. The black line separates the horizontal (left) and vertical (right) BPMs.

smaller than expected. Adding the fitted amplitudes to the CO yields positions extremes of the beam at these BPMs to be ∼20 mm. These large positions in the uncalibrated measurement region of the BPM most probably compromised the quality of the amplitude measurement at these BPMs. This bad amplitude measurement in the vertical could have been mitigated by centering the CO and checking the injection offset.

The largest contribution to the bad amplitude measurement is the number of turn-by-turn data points in one betatron oscillation. With the fractional vertical tune very close to .5, only two turns of BPM data may be collected per betatron oscillation. Two data points are hardly enough to fit an cosine oscillation. The phase of the betatron oscillation at these BPMs could be such that the oscillation maximum was never sampled for the fit. This would reduce the resulting fitted amplitude.

Although the improved model produces a larger χ^2 in the beta function compared to the baseline model, it is believed that this is due to a poor vertical amplitude measurement and not a bad improved model prediction.

VIII. LOCO AND THE IMPROVED MODEL

Now with the improved model verified as an enhanced model at the PSR operational set point and set points far away from nominal, it is time to tie up loose ends.

Although the improved model of the PSR leads to only ∼.1 radian cumulative one-turn phase difference compared with measurement, the systematic mistreatment of the vertical phase is still observable in Fig. 6. Of course this trend is much reduced compared to the results from the baseline model plotted in Fig. 2. This may be evidence that the focal lengths of the rectangular dipole edge focusing depends on the central magnet field of the bender, which agrees with the form in Eqs. (4) and (5). Operating the dipoles at a current different than that for the ray tracing calculation could yield a trend in the vertical phase difference and not the horizontal. Additionally, dipole hysteresis may be to blame for the residual systematic trend in the vertical phase difference. Nonetheless, this systematic mistreatment of the vertical phase in the model is minimal and still yields a predicted tune within .005, which is a factor of 10 better than the baseline model. A dipole magnetic field or current to edge focusing focal length conversion would enhance the model's ability to predict the vertical tune, especially for different energy beams where the magnetic fields of the PSR benders must be modified.

A final loose end of this exercise to improve the model of the PSR is the initial LOCO result, which indicated ∼−2.5% decrease in the strength of the defocusing quadrupoles[6]. The LOCO result was rejected because the 2.5% decrease in defocusing quadrupole strength was not observed as issues with the controls set point, controls read back, power supply output current, or quadrupole hysteresis. It was believed that LOCO adjusted the defocusing quadrupole strength to correct for the systematic mistreatment of the baseline model vertical phase. However, because the quadrupoles were not the accelerator element which caused the systematic vertical phase mistreatment in the model, modification of the quadrupole strengths caused the LOCO fitted model to predict beta functions worse than the baseline model, although it nailed the vertical tune prediction. This is why the LOCO fitted model was not declared an improved model.

It is of interest to verify that the modification to the edge focusing focal lengths in the improved model improves the LOCO fit for the quadrupole strengths. This test will show that the vertical phase mistreatment in the baseline model is due to incorrect edge focusing and not quadrupole strengths. LOCO is employed to fit the improved model to the measured ORM from Ref. [6]. LOCO is instructed to verify the BPM gains, corrector kicks, and the quadrupole strengths to fit the ORM. The results for the LOCO fitted quadrupole strengths are shown in Fig. 8

Supplying the improved PSR model as input, LOCO not longer suggests ∼−2.5% decrease in the defocusing quadrupole strength. LOCO does vary the quadrupole strengths minimally by ±1% to correct for the small systematic mistreatment of the vertical phase still present in the improved model. Additionally, LOCO could be trying to recover any residual quadrupole hysteresis be-

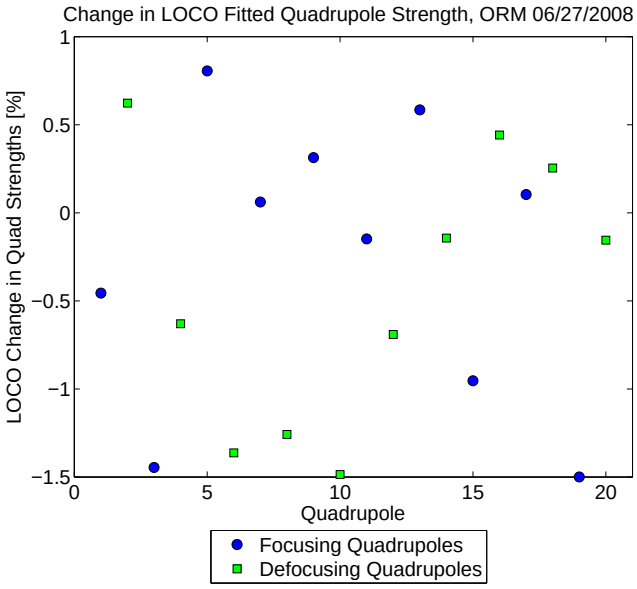

FIG. 8: (Color) LOCO fit of the quadrupole strengths from the improved PSR model to the measured ORM of Ref. [6]. The quadrupoles are number consecutively 1 through 20 as they appear in the PSR: SRQF01, SRQU01, SRQF11, ..., SRQU91.

cause the quadrupole magnet power supplies were not cycled prior to the ORM measurement.

Nonetheless, the LOCO fit produces somewhat of a null result, which indicates that the input model was correct and is further verification of the improved model.

IX. CONCLUSIONS

A ray tracing technique was employed to track particle positions through simulated 3D magnetic fields of a common 36° PSR type bender, a common PSR bender operated at 100 A less current than nominal for SRBM01, each C-magnet (SRBM11 and 12), and the merging magnet RIBM09. The rays received a vertical kick (a vertical angle change) in the fringe fields of the dipoles. Ray tracing continued for about a meter after the vertical kick allowing for a focal length of the edge focusing lens to be calculated. The focal length for each dipole calculated in this manner was related to and compared with the fringe field integral in the K. Brown model[12]. It was found that the fringe field integrals employed in the baseline model, which were calculated directly from a 3D magnetic field simulation for each bender type, produced a focal length for the edge focusing that was systematically shorter than the focal lengths calculated from the ray tracing. The largest relative difference in the edge focusing focal lengths was only .5 m and occurred for the common 36° PSR benders. Employing the fringe field integrals from the direct calculation of the 3D magnetic field simulation, which are systematically shorter than those produced by the ray tracing data, provides the addition vertical focusing in the baseline model and produces the systematic mistreatment of the vertical betatron phase and incorrect vertical tune prediction. Applying the fringe field integrals from the focal lengths calculated from the ray tracing data in the PSR model resulted in correct predictions of the vertical betatron tune.

An improved model of the PSR was created with the fringe field integrals produced from the focal lengths calculated from the ray tracing data. Additionally, the improved PSR includes the focusing effects of the fringe fields of the PSR extraction septa, which were measured in Ref. [5]. Predictions of the linear lattice functions by the improved model were compared with the predictions of the LOCO fitted model of Ref. [6], the baseline model, and the measured betatron tunes and phases[1], dispersion function[3], and beta functions[4]. The improved model predicted the linear lattice functions at least as well or better than the LOCO fitted and baseline models. This shows that the improved model is the better model at one PSR operating set point.

However, a universally improved model of the PSR is desired, so comparisons of the linear lattice function predictions of the improved model were made with the baseline model and measurement at set points far away from the nominal PSR operating set point. These comparisons were made for betatron tunes of [3.2266, 2.2192], [3.8002, 2.3826], and [2.6539, 3.5829]. At each of these different operating set points, the predictions of the improved model were closer to measurement than those of the baseline model. Thus the improved PSR model has been created and verified by measurement.

Lastly, LOCO is applied to the improved model. The LOCO fit only slightly modifies the quadrupole strengths and no longer indicates $\sim -2.5\%$ decrease in the defocusing quadrupole strength as was the results when LOCO operated on the baseline model[6]. This results shows that the quadrupole strengths in the improved model are correct.

Acknowledgments

This work was supported in part by United States Department of Energy under contract DE-AC52-06NA25396 and by grants from the US DOE under contract DE-FG02-92ER40747 and the NSF under contract NSF PHY-0852368.

Special thanks to SY Lee of Indiana University.

[1] J. Kolski, R. Macek, R. McCrady, "A RingScan Reproducibility Measurement in the Los Alamos Proton Storage Ring", LA-UR 10-05272, PSR 10-001, AOT-ABS 10-006.
[2] J. Kolski, R. McCrady, "A Beam-Based Hysteresis Measurement in the Los Alamos Proton Storage Ring", LA-UR 10-02208, PSR 10-002, AOT-ABS 10-009.
[3] J. Kolski, R. Macek, R. McCrady, "A Comparison of Two Methods to Measure the Beam Momentum in Application to Measuring the Dispersion Function in the Los Alamos Proton Storage Ring", LA-UR 10-03867, PSR 10-003, AOT-ABS 10-018.
[4] J. Kolski, R. Macek, R. McCrady, "A Measurement of the Betatron Amplitude Functions in the Los Alamos Proton Storage Ring", LA-UR 10-05104, PSR 10-004, AOT-ABS 10-020.
[5] J. Kolski, R. Macek, R. McCrady, "Beam-Based Measurements of the Magnetic Multipole Components of the Extraction Septum Fringe Fields in the Los Alamos Proton Storage Ring", LA-UR 10-05747, PSR 10-005, AOT-ABS 10-023.
[6] J. Kolski, R. Macek, R. McCrady, "Orbit Response Matrix (ORM) Analysis in the Los Alamos Proton Storage Ring", LA-UR 11-10134, PSR 11-002, AOT-ABS 11-014.
[7] J. Safranek, "Experimental determination of storage ring optics using orbit response measurements", NIM-A388 (1997) 27.
[8] Private conversations with R.J. Macek.
[9] Private conversations with F. Neri.
[10] J. Safranek, G. Portmann, A. Terebilo, "Matlab-Based LOCO", EPAC 2002, WPELE003.
[11] S.Y. Lee, "Accelerator Physics 2nd ed."
[12] K.L. Brown, SLAC Report-75, 1982.
[13] H. Grote and F.C. Iselin, "The MAD Program (Methodical Accelerator Design), Version 8.19, User's Reference Manual", CERN/SL/90-13(AP), Rev. 5.
[14] F. Neri, "psrdimad.txt", PSR Model.
[15] D. Fitzgerald, "Field Measurements for the PSR Quads and Ring Lattice Functions", PSR 89-003.
[16] D. Fitzgerald's Data CD, "LD, Beams, Magnets, Shielding", 6/16/2004.
[17] D. Barlow, "Ring Bender k1.xls".
[18] L. Rybarcyk, "PSR-Survey-layout-analysis.xls", 2006 PSR Alignment Data collected by C. Conners and G.W. Isern.
[19] S. Cousineau, "PSR_319_219.mad", PSR Model.
[20] D. Barlow, "SRBM Fringe Field.xls".
[21] D. Barlow, "SRBM01 Fringe Field.xls".
[22] D. Barlow, "SRBM11 Fringe Field.xls".
[23] D. Barlow, "SRBM12 Fringe Field.xls".
[24] D. Barlow, "RIBM09 Fringe Field.xls".